J Multimodal User Interfaces (2017) 11:67–80
DOI 10.1007/s12193-016-0230-y

ORIGINAL PAPER

Multimodal feedback for teleoperation of multiple mobile robots in an outdoor environment

Ayoung Hong[1] · **Dong Gun Lee**[2] · **Heinrich H. Bülthoff**[3,4] · **Hyoung Il Son**[5]

Received: 21 August 2015 / Accepted: 20 August 2016 / Published online: 27 August 2016

Abstract Better situational awareness helps understand remote environments and achieve better performance in the teleoperation of multiple mobile robots (e.g., a group of unmanned aerial vehicles). Visual and force feedbacks are the most common ways of perceiving the environments accurately and effectively; however, accurate and adequate sensors for global localization are impractical in outdoor environments. Lack of this information hinders situational awareness and operating performance. In this paper, a visual and force feedback method is proposed for enhancing the situational awareness of human operators in outdoor multi-robot teleoperation. Using only the robots' local information, the global view is fabricated from individual local views, and force feedback is determined by the velocity of individual units. The proposed feedback method is evaluated via two psychophysical experiments: maneuvering and searching tests using a human/hardware-in-the-loop system with simulated environments. In the tests, several quantitative measures are also proposed to assess the human operator's maneuverability and situational awareness. Results of the two experiments show that the proposed multimodal feedback enhances only situational awareness of the operator.

Keywords Multimodal feedback · Multi-robot systems · Psychophysical evaluation · Bilateral teleoperation · Outdoor environment

1 Introduction

Autonomous mobile robots have been recognized as promising solutions for surveillance, search and rescue problems in disaster regions, and exploration in hazardous regions. The advantages of autonomous mobile robots become more significant if a group of them is considered because of better performance in terms of simultaneous spatial domain coverage, better affordability, and robustness against single-point fillers [1]. Nevertheless, when the tasks become extremely complex and high-level cognitive-based decisions are required (e.g., the exploration of dynamic, unstructured, and unpredictable environments in search and rescue applications), full autonomy is still far from being reached and human intervention/assistance is necessary for better performance [2–4]. In this context, bilateral teleoperation systems, where a human operator commands remote robots through an interface and receives informative feedback cues to achieve awareness of the remote environment, allow human operators to exploit their intelligence to solve complex tasks with currently available robots [5].

✉ Hyoung Il Son
hison@jnu.ac.kr

Ayoung Hong
ahong@ethz.ch

Dong Gun Lee
firstop@kaist.ac.kr

Heinrich H. Bülthoff
hhb@tuebingen.mpg.de

1 Institute of Robotics and Intelligent Systems, ETH Zurich, 8092 Zurich, Switzerland

2 Institute of Industrial Technology, Samsung Heavy Industries, Daejeon 305-380, Korea

3 Max Planck Institute for Biological Cybernetics, Spemannstraße 38, 72076 Tübingen, Germany

4 Department of Brain and Cognitive Engineering, Korea University, Anam-dong, Seongbuk-gu, Seoul 136-713, Korea

5 Department of Rural and Biosystems Engineering, Chonnam National University, 77 Yongbong-ro, Buk-gu, Gwangju 550-757, Republic of Korea

Visual and force feedback are the most common ways of perceiving environments accurately and effectively; these use vision systems and haptic devices, respectively. In outdoor environments, however, it is difficult to use adequate/accurate sensors (e.g., global vision and localization systems outdoors) for control of multi-robot systems (e.g., maintaining formation) and haptic feedback for the remote environment when using multiple remote robots. A camera mounted on mobile robots could be a good solution for visual feedback and robot localization in outdoor environments [6,7]. In fact, it is easy to use the on-board camera because it is installed in most mobile robots owing to its efficiency in terms of light weight, low energy consumption, and low cost.

There is, however, limited visual information on remote environments during outdoor teleoperation with only an on-board camera owing to its limited field of view (FOV). In the case of multi-robot teleoperation, a human operator's situational awareness could be enhanced through combined visual information from multiple local cameras. Nevertheless, the human operator still needs information about the global status of a multi-robot system (e.g., relative distances between robots and their formation) for better situational awareness of remote environments in order to achieve good performance with multiple robots. The operator could imagine the global status of a multi-robot system by combining multiple local views from the on-board cameras in her/his brain. However, if the number of remote robots is increased, the cognitive load required for the operator to synthesize the global status is increased exponentially.

From this perspective, there is a need for a better visual feedback method to enhance the teleoperator's situational awareness of the local and global status of a multi-robot team and the outdoor environment with lower cognitive load. Furthermore, it is expected that force feedback will give additional benefit to visual feedback as some authors have found merit in force feedback for indoor teleoperation of multiple unmanned aerial vehicles (UAVs) [8].

1.1 Related work

To enhance the human operator's situational awareness of remote environments, people have proposed multi-modal interfaces [9–11], visual-vestibular feedback [12], artificial force field feedback [7], haptic cue feedback [13,14], and virtual reality displays [10,15–17].

Chen et al. summarized the causes of performance diminution: video image bandwidth, time lag, frame rate limitation, lack of proprioception, frame of reference, two-dimensional views, attention switches, and motion effects, which result in the lack of an operator's situation awareness. To solve these problems, multimodal interfaces and various predictive and decision support systems were suggested in [9]. Multimodal interfaces provide a variety of control modalities and visualizations (video- and map-centric) [10,11]. These interfaces have been developed and have been applied in volcano exploration, satellite servicing, telehomecare, unmanned aerial system, and to operate mobile robots with adjustable autonomy [10]. In addition to multimodal feedback, vestibular feedback, a type of kinesthetic feedback, has been proposed and integrated with visual feedback from cameras on board slave robots to improve the situational awareness of a master operator [12]. To prevent UAV collisions, a novel virtual force field for haptic feedback is used to safely reduce the number of collisions with obstacles by providing haptic feedback to an operator when visual information is insufficient for perceiving environment information [7]. In addition, design of haptic cues to increase operators' perceptual sensitivity was further researched in [5,13,14]. Haptic feedback for multiple UAV teleoperation systems was designed by using velocity information and proximity to obstacles to optimize the environmental awareness of an operator [5,13].

As a demanding component of multimodal feedback, visual feedback was more emphasized in [10,15–17], and several ways for designing visual feedback are introduced. Using RGB-D sensors, global 3D environment maps were visualized to reduce search times for objects and realize fewer collisions with less operator work load and improved situation awareness [15]. In [16], navigation maps were displayed virtually in a 3D reality display by combining with video from cameras on the slave robots along with robot pose information. This method showed better performance in comparison with other cases: 2D or 3D interfaces; with or without navigation maps; and with or without camera videos. In addition, mixed-reality visualization modalities were proposed using video- and map-centric user interfaces so that operators understand sufficiently the remote environment and achieve high level performances, in terms of completion time, the distance traveled by the robot, and the number of commands executed by the operator for each task [10]. Furthermore, a photorealistic rendering model for a mixed virtual reality interface was proposed to overcome limitations such as dense obstacles, low video quality, and wireless links [17].

Performance metrics were also suggested to evaluate the effectiveness of the proposed methods for the enhancement of human operators' situational awareness in remote environments. General performance metrics for task-oriented human–robot interaction have been discussed in terms of the system, operator, and robot performance [18]. Following this research, metrics (neglect tolerance, robot attention demand, fan-out, and interaction effort) were identified for task-oriented interaction with a fuzzy temporal model to evaluate human trust in automation [19]. In [19], another fuzzy temporal-based model was presented to evaluate human reliability during interaction time. This model accommodated multi-robot scenarios by considering sequential and paral-

lel robot cooperation schemes with varying levels of task dependency. Human operators' situational awareness was investigated with task performance [20]. In [20], several methods of measuring the situational awareness of human operators were compared for urban search and rescue tasks with defined measures: total searched area, mission time, reward for bringing the robot back safely, and rewarding large coverage.

In addition, performance evaluation of human–robot interaction was carried out in various applications [5,21–24]. For bilateral teleoperation of multiple UAVs, a human-centered evaluation was used to show the performance of haptic cues via a master device to benefit maneuverability and perceptual sensitivity, and several metrics were defined to evaluate these two measures [5]. In multi-user teleoperation for mobile manipulators at unmanned offshore plants, a human-centered evaluation was also performed to evaluate the benefits of the proposed multi-user teleoperation system in terms of task completion time and interaction forces, and several quantitative metrics were defined for the evaluation [21]. For space investigations, a remote human–robot operation system was proposed for carrying out tasks such as navigation to a location and photographing images [22]. Robot performance was measured during reconnaissance operations by monitoring robot telemetry and computing performance metrics in real time from the data. In order to assess this, measures were proposed in terms of time, team productivity, and task success. In a practical palpation and perception of the stiffness task, a multi-dimensional measure of transparency, which takes into account the human operator, was introduced, consisting of three components: perceptual transparency, local motor transparency, and remote motor transparency [23]. Using these measures, gains that ensure perfect perceptual and remote motor transparency of the measures while maintaining stability were derived. Moreover, in [24], a teleoperation system for multiple social robots was proposed where an operator must perform auditory multitasking to assist multiple interactions simultaneously. To describe and predict this robot performance, three task difficulty metrics (recognition accuracy, situation coverage, and critical time ratio) were defined.

1.2 Objective and outline

In this paper, we propose a multimodal (i.e., visual and force) feedback method for teleoperation of multiple mobile robots (i.e., UAVs) in outdoor environments. Visual and force feedback are produced, based on the bearing-only formation control presented in [25], using only the bearing information of inter-UAVs from local UAV cameras and velocities. The proposed multimodal feedback is evaluated via two psychophysical experiments (namely, maneuvering and searching tests) to show its effectiveness in enhancing teleoperator performance with better situational awareness. The experiments were conducted using a human/hardware-in-the-loop system with a haptic device and a physically realistic simulation of multi-UAVs and environments. Several measures are also presented to analyze experimental results in a rigorous way. This paper is extended from our previous work [26] by presenting full experimental results with in-depth analysis and discussion of the results.

The rest of the paper is organized as follows. The bearing-only formation control for outdoor teleoperation of multiple robots is reviewed in Sect. 2. Then, in Sect. 3, the multimodal feedback method is proposed based on teleoperation control. After presenting the experimental method in Sect. 4, the performance measure and data analysis method is discussed in Sect. 5. Following this, experimental results are reported and discussed in Sect. 6. Finally, the paper is concluded in Sect. 7.

2 Teleoperation of outdoor multi-UAVs

In this paper, we develop multimodal feedback for teleoperation of multiple UAVs in outdoor environments based on [25]. Hereafter, we briefly recapitulate the modeling and control of bearing formations of multiple UAVs discussed in [25] and refer the reader to the background with further details.

The control objective of multi-UAVs is to maintain autonomously the desired formation of all agents (i.e., UAVs) while allowing the operator to steer the overall motion of the formation via a haptic device. In this application, the absolute positions and yaw angles of agents have limited reliability using calibrated cameras, inertial measurement units (IMUs), and compasses. This is because yaw angles are difficult to measure using IMUs, and compasses do not work well indoors or close to strong magnetic fields. Therefore, the relative bearing is used to keep the agents' bearing formation, in practice.

Definition 1 The *relative bearing*, between agents i and j, is defined as

$$\beta_{ij} = {}^{i}R\frac{p_j - p_i}{\|p_j - p_i\|} \tag{1}$$

where $i, j \in \{1, \ldots, N\}$, ${}^{i}R$ is the canonical rotation matrix of the agent i about the Z axis, and p_i and p_j are the position configuration of agent i and j, respectively.

To achieve a feasible motion of agents, the linear velocity and yaw-rate of body frame, $u \in \mathbb{R}^3$ and $w \in \mathbb{R}$ are considered as control inputs. The control inputs to the agent i is orthogonally divided into two as follows.

$$(u_i, \omega_i) = (u_i^h, \omega_i^h) + (u_i^f, \omega_i^f) \tag{2}$$

The term (u_i^h, ω_i^h) is the *high-level steering control* input responsible for steering the collective motion of the UAV group while preserving relative bearings. Therefore, human operator inputs are used in this first term to control translation and expansion of the formation. The second term (u_i^f, ω_i^f) is the *bearing-formation control* input used for converging the relative bearing (β_{ij}) to the desired bearing formation (β_{ij}^d). The first and second terms are illustrated in Sects. 2.1 and 2.2, respectively.

2.1 High-level steering control

The control law $\{(u_i^h, \omega_i^h)\}_{i=1,\ldots,N}$ allows the human operator to control the motion of the agents. It is assumed that the operator controls agent 1's linear velocity ($v \in \mathbb{R}^3$) and that the expansion rate of the formation ($s \in \mathbb{R}$).

Definition 2 The *high-level steering control law* is defined as

$$\begin{cases} u_i^h = {}^i R_1 v - s\gamma_{12i}\beta_{i1} + \omega\delta_{12}\gamma_{12i} S\beta_{i1} \\ \omega_i^h = \omega \end{cases} \tag{3}$$

In the high-level steering control law, ${}^i R_1$ is the rotational matrix between agents i and 1, S is the skew-matrix of e_3 ($e_3 = [0\ 0\ 1]^T$), and $\gamma_{12i} := \frac{\delta_{1i}}{\delta_{12}}$. Note that Eq. (3) requires δ_{12} in order to implement correctly a synchronized group rotation. If δ_{12} is not available, then $\hat{\delta}_{12}$, an arbitrary initial guess, can be used; but this causes transition of the bearing formation. In this case, feedback control for *bearing formation control* in Eq. (4) will maintain errors of the formation that are bounded.

Remark 1 The motion control law allows the velocity command to expand the limited workspace of the operator into the unlimited workspace of the agents.

2.2 Bearing formation control

Figure 1 presents the concept of the bearing formation control law visually for three agents. The control law $\{(u_i^f, \omega_i^f)\}_{i=1,\ldots,N}$ has to achieve a set of feasible desired bearings $\{\beta_{ij}^d\}_{(i,j)\in\mathcal{N}} \in \mathbb{R}^3$ where $\mathcal{N} = \{(i,j) \in \{1,\ldots,N\}^2 \mid i \neq j\}$ using only the measured relative-bearings $\{\beta_{ij}\}_{(i,j)\in\mathcal{N}} \in \mathbb{R}^3$. This means that the control steers β_{ij} towards β_{ij}^d and the distances $\{\delta_{ij}\}_{(i,j)\in\mathcal{N}}$ towards a constant non-zero value in Fig. 1.

Definition 3 The *bearing-formation control law* is defined as

$$\begin{cases} u_i^f = K_p^i R_1(\gamma_{12i}^d \beta_{1i}^d - \gamma_{12i}\beta_{1i}) \\ \omega_i^f = K_\omega[{}^1 R_i^d R_1 - {}^1 R_i R_1^d]_{\vee,3} \end{cases} \tag{4}$$

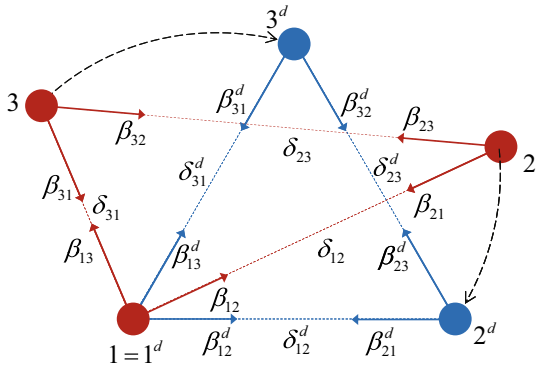

Fig. 1 Schematic of bearing-only formation control with three agents. Agents 2 and 3 are approaching the desired position 2^d and 3^d, respectively, by bringing the bearings (β_{12} and β_{13}) towards the desired values (β_{12}^d and β_{13}^d) and the distances (δ_{12} and δ_{13}) towards δ_{12}^d and δ_{13}^d

where $i = 3, \ldots, N$ and K_p, $K_\omega > 0$ are positive gains, and $[A]_{\vee,3}$ is the third component of the vector associated to a skew-symmetric matrix A.

In the bearing-formation control law, the superscript d represents the desired parameter.

Note that Eq. (4) is singular if *all* the positions of the agents are aligned on the same line. To avoid from this singularity, a practical workaround should be applied in order not to fall into its neighborhood.

3 Multimodal feedback

3.1 Visual feedback

The local views captured by the on-board cameras (hereafter, referred to as *local view feedback*) are shown in Fig. 2a. From this local view feedback, we can obtain the global bearing formation of all UAVs in Fig. 2b using the control laws explained in Sect. 2. Based on the local views, the visual feedback shown in Fig. 3 (hereafter, referred to as *fabricated global view feedback*) is fabricated to enhance the quality of visual feedback with additional information on the formation and direction of motion of the UAVs (see Fig. 3b). All (real) local views of the UAVs are also given in a certain order in the fabricated global view feedback, as shown in Fig. 3a. The detailed fabrication procedure for visual feedback is presented as follows.

For the fabrication of visual feedback, first, we define the direction of motion of N UAVs, $\bar{v}_s \in \mathbb{R}^3$ as $\frac{1}{N}\sum_{i=1}^N v_s^i$. The angle $\theta^i \in \mathbb{R}^3$ between the direction of the camera on the i-th UAV ($\beta^i \in \mathbb{R}^3$) and the average direction of motion of N UAVs ($\bar{v}_s$) is then obtained as follows (see Fig. 4).

$$\theta^i = \arccos\left(\frac{\beta^i \cdot \bar{v}_s}{\|\beta^i\|\|\bar{v}_s\|}\right) \tag{5}$$

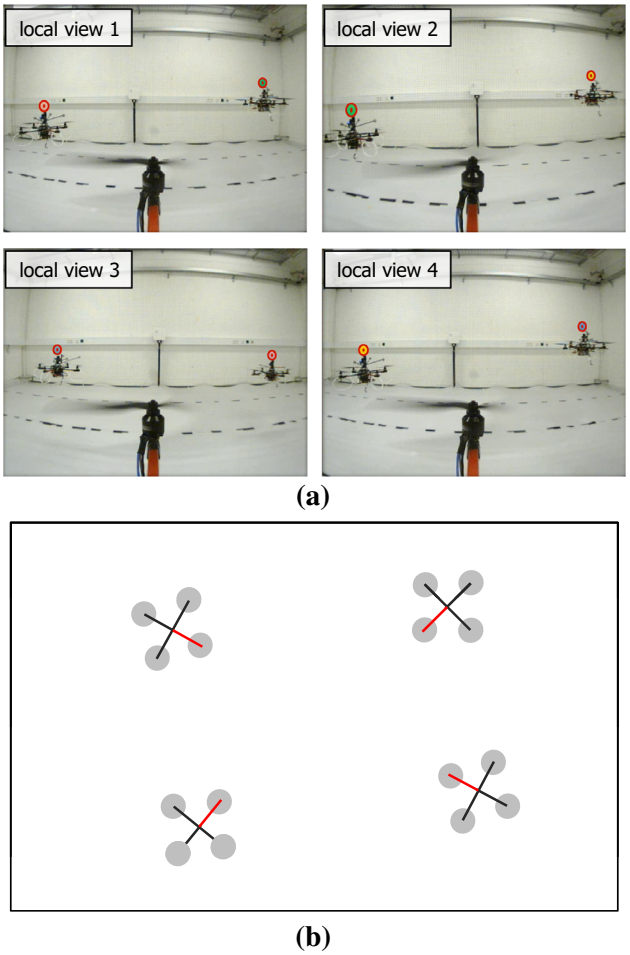

Fig. 2 Local view feedback. **a** Real local views from on-board cameras in UAVs. **b** Fabricated formation information of UAVs using bearing-only formation control

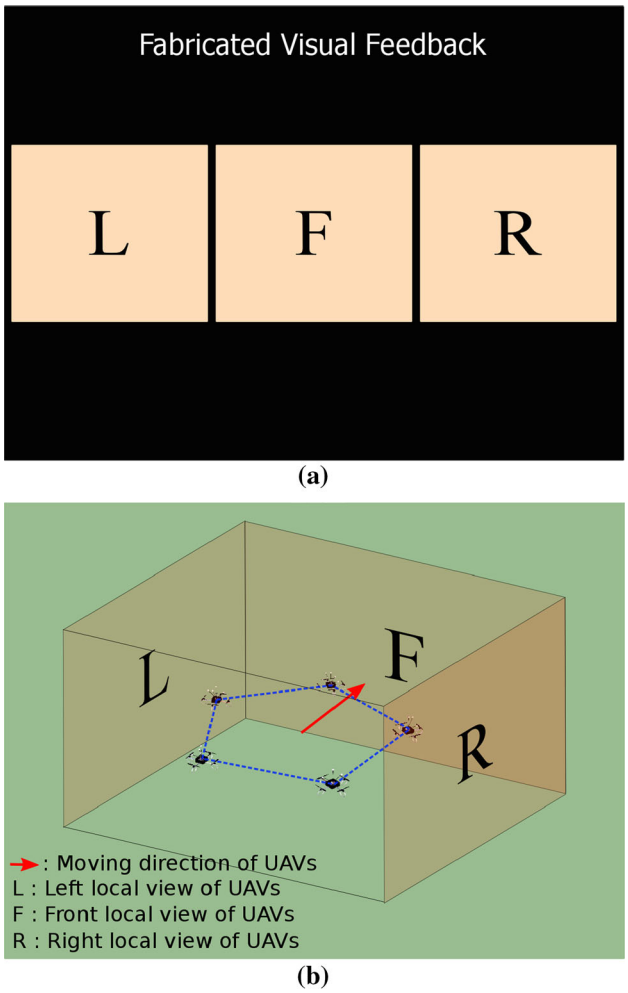

Fig. 3 Fabricated global view feedback with direction information. **a** Rearranged real local views. **b** UAV formation and direction of motion information

Definition 4 From (5), *primary local view* is defined, which satisfies

$$\theta^{primary} = \arg\min_{i \in \mathcal{N}}(\theta^i) \tag{6}$$

where $\mathcal{N}$ denotes the set of $i \in \{1, \ldots, N\}$.

After defining the primary local view, each remaining local view is arranged according to the magnitude of its angle θ^i (e.g., see Fig. 4).

In the next step, we present the primary local view in the center, and the other views are presented in the right and left areas according to their order (i.e., the magnitude of θ^i) (see Fig. 3a). In addition, the global formation of the UAVs (i.e., Fig. 2b) is also presented with $\bar{v}_s$ (see Fig. 3b). With the re-arranged real local views and the fabricated global view, therefore, human operators can obtain additional local information (i.e., the direction of the cameras with respect to the UAVs) and new global information (i.e., the formation of the direction of movement for the UAVs) with reduced cognitive load.

Remark 2 Note that if $\bar{v}_s$ changes very frequently, then the display order of the local views is also changed very quickly. This could cause visual confusion for the operator, and the quality of visual feedback might be decreased. To prevent this, we use a threshold when we find $\theta^{primary}$ and ordering θ^i.

Remark 3 In the paper, we define *ideal global view feedback* as visual feedback in an exo-centric view of the multi-robot system by employing a virtual external camera; this is almost impossible in practice. The ideal global view feedback could be available in cases of (multi-robot) teleoperations in indoor environments using an external camera situated in the environments (e.g., on a wall) (e.g., see Fig. 5) [3,4].

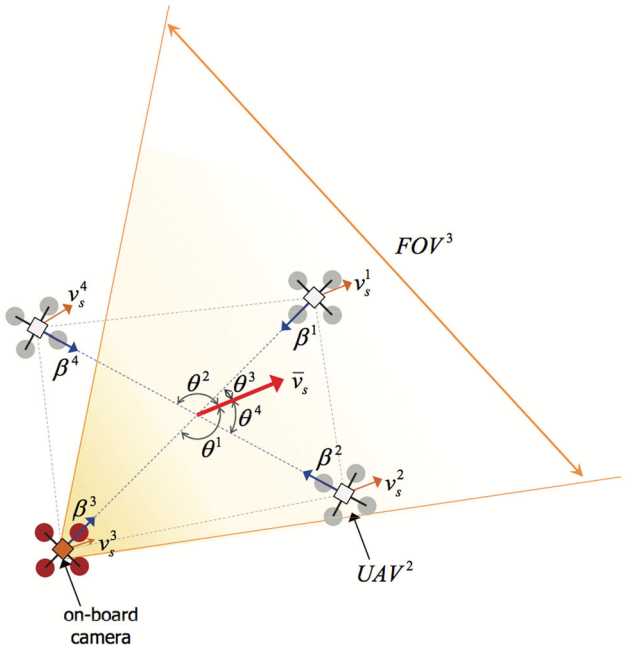

Fig. 4 Schematic for fabrication of visual feedback

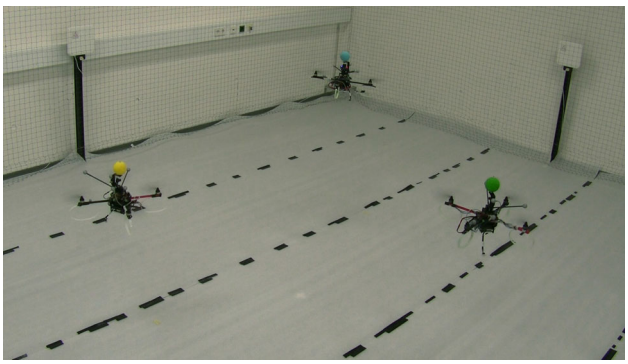

Fig. 5 Ideal global view in an indoor environment

3.2 Force feedback

We use a 3-degree-of-freedom (3-DOF) haptic feedback device to control the motion of the UAVs. Note that, in this paper, the expansion of the UAVs' formation is not considered (i.e., s in (3) was set to zero, and was controlled by a second haptic device in [25]). The haptic device is modeled as

$$M(x)\ddot{x} + C(x, \dot{x})\dot{x} = \tau + f_h \tag{7}$$

where $x \in \mathbb{R}^3$ is the configuration, $M(x) \in \mathbb{R}^{3\times3}$ and $C(x, \dot{x}) \in \mathbb{R}^{3\times3}$ are the inertia and Coriolis matrix, respectively, and $\tau \in \mathbb{R}^3$ and $f_h \in \mathbb{R}^3$ are the control input and the human input force, respectively. The velocity control input v in (3) from the human operator is defined as

$$v = \lambda x \tag{8}$$

where $\lambda > 0$ denotes a velocity scaling factor.

We design the haptic cue τ as proportional to the velocity tracking error e as

$$\tau = -B\dot{x} - Ke \tag{9}$$

where

$$\begin{aligned} e &= x - \dot{q} \\ &= x - \frac{1}{\lambda N}\sum_{i=1}^{N}(\gamma_{12i} R_i \beta_{i1} + R_i \dot{q}_i). \end{aligned} \tag{10}$$

Here, B and K are the positive definite matrixes to stabilize the master device and scale the velocity tracking error. The velocity tracking error is obtained with the haptic device configuration x and the actual velocity of agents $\dot{q}$ [27]. The actual motion of the i-th UAV is denoted as $q_i = (p_i, \psi_i)$ with the centroid and the yaw angle, and $\dot{q}_i$ is the actual velocity of the i-th agent. This haptic cue, generally, gives inertial information for the UAVs [5].

Remark 4 The matrix K represents a gain related with the magnitude of force feedback to human operator. And, in this paper, we didn't consider a specific method to guarantee system stability. Instead, we use a simple approach to maintaining the stability by adding the damping value (i.e., $B\dot{x}$) although there is a decrease in a quality of the force feedback. To improve the quality, well-developed methods such as passivity observer/passivity approach [28], passive-set-position-modulation framework [29], and port-hamiltonian approach [30] could be applied to modify (9). For more details about the selection of K and B, please refer [5].

4 Experimental method

4.1 Participants

Seventeen people from the experiment database for the Max Planck Campus Tübingen [31], participated in two tests on maneuverability and situational awareness. They were paid approximately 15 Euros to take part in this study, depending on the experiment time. All participants possessed normal eyesight and had no physical disabilities. Participants were instructed to use their dominant hand to manipulate the haptic device and to use the other hand to control the joystick.

For the maneuvering test, all participants accomplished the task for three different visual feedback methods, while for the searching test, two people did not manage to complete the task with the real local view and ideal global view because of an unexpected system shutdown. Experimental data from these two people were excluded from data analysis on the searching test.

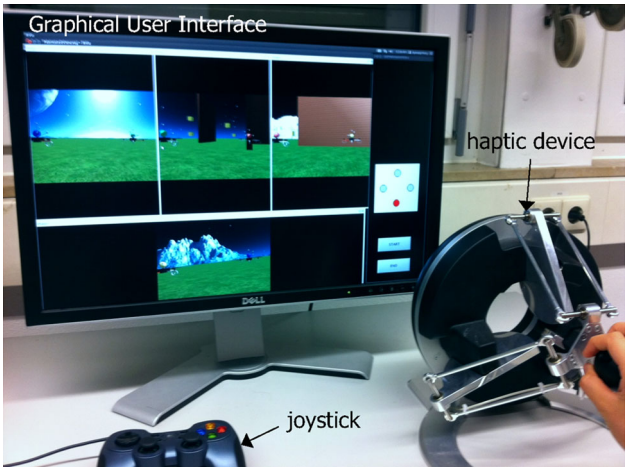

Fig. 6 Experimental setup: a graphical user interface with two input devices; Omega 3 haptic device and joystick

4.2 Apparatus

Participants ran experiments with two input devices (a haptic device and a joystick) while looking at a graphical user interface displayed on a monitor as shown in Fig. 6. They used the haptic device to maneuver a swarm of UAVs (i.e., control input v in (3)), and the joystick to rotate them (i.e., control input w in (3)) and commanded the land-on/off in the virtual environment.

A commercial haptic device, Omega 3, was used as the haptic master; this is a 3-DOF haptic device with 3 translational actuated axes. The update rate for the device is about 2.5 kHz on a dedicated Linux machine.

The UAVs and environments were simulated based on the Ogre3D engine (for 3D rendering and computational geometry computations) and PhysX libraries (for physical interaction between the UAVs and virtual environments) [32]. The four UAVs were always maintained in a rectangular formation with inter-UAV distances of about 2.1 m (i.e., δ^d). The simulation runs at 50 Hz; therefore, this restrains the communication rate between the haptic device and virtual UAVs.

4.3 Visual information presentation

The visual feedback methods for the real local view, the proposed fabricated global view, and the ideal global view are presented in Fig. 7.

For the real local view, views from each of the UAVs were positioned without predetermined order (see Fig. 7a) and thus, perception of the direction of motion and formation of the swarm of UAVs is not explicit without further information. On the other hand, the ideal global view, which is hardly feasible in outdoor environments, was implemented with a virtual camera behind and above the swarm of UAVs. Therefore, the formation of the UAVs was exposed in the view (see Fig. 7c).

The proposed fabricated global view was implemented by presenting views from each of the UAVs in a determined order, as described in Sect. 3.1 (see Fig. 7b). Three images on the upper line show the leftmost, front, and right views for the direction of motion of swarm of UAVs, respectively, and the image on the lower line shows the rearmost view like the view in vehicle rear-view mirrors. Additionally, the formation of the UAVs was presented, displaying one UAV with the primary local view in red.

4.4 Procedure

The experiments were started with the ideal global view feedback and the order of two other blocks (i.e., the real local view and the fabricated global view feedbacks) were chosen randomly for each subject. The proposed force feedback was given for all visual feedback methods.

4.4.1 Maneuvering test

Subjects should maneuver the multi-UAV system to follow a target that moves along a predefined trajectory from a start position to a target position, as shown in Fig. 8a. We have five trajectories in total; one straight trajectory, two semicircular trajectories, and two sinusoidal trajectories. All trajectories are parameterized in time t and are defined as follows.

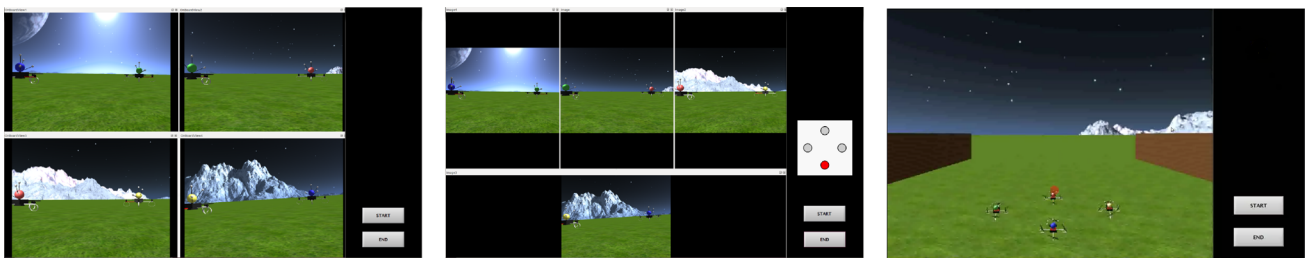

Fig. 7 Implemented visual feedback methods. **a** Real local view. **b** Fabricated global view. **c** Ideal global view

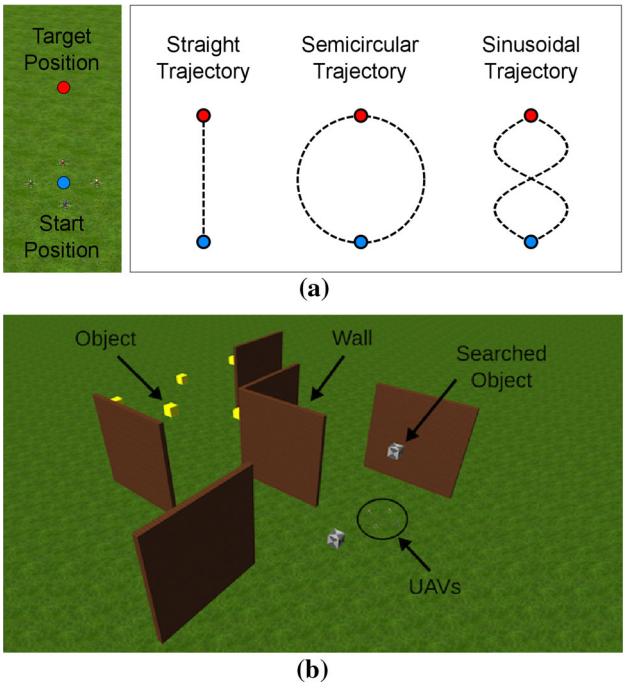

Fig. 8 Experiment layouts. **a** Maneuvering test: the subject maneuvers UAVs to follow a moving target, from the start position to the target position. The moving target follows one of trajectories. **b** Searching test: the subject searches for objects in the space

- Straight trajectory:

$$\begin{cases} x(t) = Lt/T_{st} \\ y(t) = 0 \end{cases} \tag{11}$$

- Semicircular trajectories:

$$\begin{cases} x(t) = \dfrac{L}{2}\left(1 - cos\left(\pi t/T_{sc}\right)\right) \\ y(t) = -\dfrac{L}{2} sin\left(\pi t/T_{sc}\right) \end{cases} \tag{12}$$

$$\begin{cases} x(t) = \dfrac{L}{2}\left(1 - cos\left(\pi t/T_{sc}\right)\right) \\ y(t) = \dfrac{L}{2} sin\left(\pi t/T_{sc}\right) \end{cases} \tag{13}$$

- Sinusoidal trajectories:

$$\begin{cases} x(t) = Lt/T_{si} \\ y(t) = -\dfrac{L}{2} sin\left(2\pi t/T_{si}\right) \end{cases} \tag{14}$$

$$\begin{cases} x(t) = Lt/T_{si}t \\ y(t) = \dfrac{L}{2} sin\left(2\pi t/T_{si}\right) \end{cases} \tag{15}$$

T_{st}, T_{sc}, and T_{si} are the time duration for straight, semicircular, and sinusoidal trajectories, respectively, and L is the distance between the start position and the target position. In this experiment, $T_{st} = 20$ s and $T_{sc} = T_{si} = 40$ s. We only considered horizontal movements (i.e., x- and y-axis movements in the plane) to ease the experiment so that the height of the UAVs (i.e., z-axis movement) was constant.

Within each visual feedback block, two trials for five trajectories (in total ten trials) proceeded randomly without interruption. Blue, yellow, and red buttons were displayed accordingly to indicate to participants which state they are in: a blue sign indicated that a new trial was ready, allowing participants to push the blue button on the joystick to launch UAVs; a yellow sign meant that the swarm of UAVs was ready to be maneuvered using the haptic device to follow the virtual target; and a red sign informed that the ten trials were finished.

4.4.2 Searching test

Participants controlled a multi-UAV system to find randomly positioned objects in a space. In a $50 \times 50 \times 10$ m^3 room, there were ten objects (1 m^3 cubes) and six walls, which were considered obstacles to the multi-UAV system (see Fig. 8b).

Prior to the beginning of the experiment, the subjects were told that there were several objects to find (but the exact number of objects was not given) and were given a certain amount of time to examine the sample virtual environment. The experiment started at a fixed initial point for all visual feedback methods. By controlling the multi-UAV system, the participants were required to do their best in finding the objects as soon as possible. If the center of the multi-UAV system was within 2 m of the object, the object was marked in a different color. Once participants found all the objects or the time limit was reached (in the test, 10 min), the experiment was ended.

5 Performance measures and analysis

5.1 Maneuverability

We proposed maneuverability as an assessment of the operator's ease in maneuvering slave robots in order to achieve accurate tracking performance in [5,14]. The maneuverability is defined as the frequency response of the intended-force input from the human operator, f_h, as an input, and the position tracking error as an output. The cross-correlation between the actual path, $\bar{x}_s(t)$, and the desired path, $x_d(t)$, are suggested in order to estimate the position-tracking error across the overall maneuvering time. Here, the actual path $\bar{x}_s(t)$, is defined with the geometrical centeroid of multi-UAVs formations as $\bar{x}_s = (1/N)\Sigma_{i=1}^{N} x_i$.

Definition 5 The *maneuverability* function is defined as

$$\Phi_{maneuv}(s) = \frac{CC_{position}(s)}{f_h(s)} \tag{16}$$

where

$$CC_{position} = \frac{\int_0^T \bar{x}_s(t) \cdot x_d(t)dt}{\sqrt{\int_0^T \bar{x}_s^2(t)dt}\sqrt{\int_0^T x_d^2(t)dt}} \tag{17}$$

for teleoperation systems with human force inputs f_h.

As proposed in [5,14], in this paper, the ± 3 dB bandwidth and H_2 norm of Φ_{maneuv} are defined as performance metrics to observe how well the slave robots follow the desired path and also, the degree of system sensitivity with respect to human force input.

5.2 Situational awareness

In our previous works [5,13], we evaluated the operator's situational awareness using the just noticeable difference (JND) [33]. It is, however, difficult to measure the JND of visual stimuli; therefore, in this paper, we define several task-dependent metrics to evaluate situational awareness based on [18,20]. Because the purpose of our tasks is to move a group of robots between certain points and to understand remote environments, the metrics are defined in terms of two task categories: situational awareness of navigation and perception. In the following paragraphs, the metrics that we defined and relations between them and situational awareness are addressed.

In terms of navigation and perception, we suggest task performance as an implicit method to express situational awareness based on [20]. Task performance, P_{TP}, is described with five metrics: completion time (P_{CT}), ratio of covered area (P_{CA}), ratio of search objects over total objects (P_{SO}), reward for safe return (P_{SR}), and large coverage area (P_{LA}). Mathematically, the proposed metrics are defined as follows and the required raw data for the metrics are summarized in Table 1.

Navigation is a basic task for the operation of mobile robots, which requires determining where the robots are, where they should be located, and how they interact with the environment (e.g., obstacles). During navigation, obstacles are often encountered, and robots try to avoid them. Types of situational awareness in navigation are divided into two: how fast and how well the task is accomplished. First, to measure time efficiency, the metric of completion time (P_{CT}) is defined. Second, to measure effectiveness, i.e., how well the task is done, metrics are designed for how widely robots cover the area and how successfully they avoid obstacles. For robot coverage, the metric for the ratio of covered area (P_{CA}) is defined. In addition, the metric for reward for large coverage area (P_{LA}) is designed to reward when more than 80 % of the total areas are covered. In this complex task, someone who focuses more on covering area than for searching objects must receive proper scores according to P_{LA}. Even though some participants experience difficulty in covering large areas or finding search objects, their scores should be compensated for safety control if they never collide with obstacles. P_{SR} is defined for safety performance regarding navigation.

On the other hand, the perception task focuses on how well human operators understand the remote environments of the mobile robots. Performing our task requires inferring the target objects and environments through perception of sensor data and haptic guides. Using their perception, operators judge how to control robots to find objects or avoid obstacles. For our task, P_{SO} is suitably defined as a detection measure.

Definition 6 The metric for *completion time* is

$$P_{CT} := \int_0^{t_f} dt. \tag{18}$$

where t_f is the finishing time of the experiment.

Definition 7 The metric for the *ratio of covered area* is

$$P_{CA} := \frac{\int_0^{t_f} A(t)dt}{A_{total}}. \tag{19}$$

where A_{total} is the whole area explored by the remote robots.

Table 1 Task-dependent metrics for situational awareness and required raw data

Task	Item	Acquired	Metrics
Navigation	1. Robot position and orientation	Raw data	
	2. Trajectory	1	
	3. Coverage of area	2	P_{CA}, P_{LA}
	4. Number of collisions with obstacles	2	P_{SR}
	5. Elapsed time	Raw data	P_{CT}
	6. Remaining time	4	
Perception	7. Number of search objects	1	P_{SO}
	8. Number of missed objects	6	
	9. Time to complete the task	4	

Definition 8 The metric for the *ratio of search objects over total objects* is

$$P_{SO} := \frac{\int_0^{t_f} \sigma_i(t)dt}{N_{obj}} \tag{20}$$

where $\sigma_i = \begin{cases} 1 & \text{if undetected object } O_i,\ i \in \{1, \ldots, N_{obj}\} \\ & \text{is searched} \\ 0 & \text{elsewhere.} \end{cases}$

N_{obj} is the number of object to be searched.

Definition 9 The metric for *reward for safe return of robots is*

$$P_{SR} := \begin{cases} 1 & \text{if robots are returned safely} \\ 0 & \text{elsewhere.} \end{cases} \tag{21}$$

Definition 10 The metric for *reward for large coverage area* is

$$P_{LA} := \begin{cases} 1 & \text{if } P_{CA} \geq 0.8 \\ 0 & \text{elsewhere.} \end{cases} \tag{22}$$

Finally,

Definition 11 Task performance is defined as

$$P_{TP} := \left(\frac{P_{CA}}{P_{CT}} \times k_n^2 + \frac{P_{SO}}{P_{CT}} \times k_n^3 + P_{SR} + P_{LA} \right) \times k_n^1 \tag{23}$$

where k_n^1, k_n^2, and k_n^3 are factors to normalize P_{TP}, P_{CA}, and P_{SO} between zero to unity.

Unifying the five measures, P_{TP} is defined as a combination of them by weighting with coefficients (k_n^1, k_n^2, and k_n^3). In P_{TP}, the effectiveness of the search area and objects is obtained by dividing P_{CA} and P_{SO} by P_{CT}. Therefore, if more area is covered or more objects are found in a shorter time, a participant usually gets a higher score. After all, larger values of P_{TP} mean better performance. For the other metrics, smaller values of P_{CT} mean better performance, but for the other measures (i.e., P_{CA}, P_{SO}, P_{SR}, and P_{LA}), larger values represent better performance.

5.3 Data analysis

Two metrics, the bandwidth and the H_2 norm of the maneuverability frequency response (Φ_{maneuv}), served as performance metrics for maneuverability. These measures were separately computed for x- and y-axis components. Φ_{maneuv} was calculated by applying the empirical transfer function estimator [5], using a second-order low-pass filter (W_{low}) with a cut-off frequency of 8 Hz as follows.

$$\|\Phi_{maneuv}\|_2 = \left\| W_{low} \frac{CC_{position}}{f_h} \right\|_2 \tag{24}$$

Here, human force (f_h) is defined as τ, which is the master control force given by the force feedback algorithm (see (7)).

In the searching test, task-dependent metrics were calculated from raw data; positions and orientations of the UAVs were obtained by the virtual sensors and the timer in the simulations. The metric for completion time (P_{CT}) can be obtained directly from raw data of the timer. On the other hand, other task-dependent metrics (i.e., P_{CA}, P_{SO}, P_{SR}, and P_{LA}) proposed in Sect. 5.2 were computed with the positions of UAVs and P_{CT} (see Table 1).

The whole area to be explored by the multi-robot system was the size of the virtual room in the searching test. We computed the portion of the room explored by the multi-UAV system. Successfully finding objects was determined based on the trajectory profile of the multi-UAV system. When the distance between an object and the center of the multi-UAV system was less than 2 m, the object was marked. A reward for safe return was only given when subjects finished the experiment without any incidents such as formation loss, collisions, or failure to find all the objects.

The normalizing factors, k_n^1, k_n^2, and k_n^3, were calculated using the following normalization method with smoothing parameter $a = 50$.

$$k_n^i = \frac{1}{2} \left(1 - \frac{P_i}{\sqrt{P_i^2 + a}} \right) \tag{25}$$

where $i = 1, 2, 3$ and P_i is the maximum value of the performance metrics related to k_n^i.

Finally, a two-way analysis of variance (ANOVA) test was exploited for statistical analysis and to formally determine whether there is statistically significant difference (i.e., p value <0.05) in performance measures.

6 Experimental results and discussion

6.1 Experimental results

6.1.1 Maneuverability

Experimental results of the maneuverability test are summarized in Figs. 9, 10, and 11 for three different performance metrics of maneuverability, respectively. In addition, Table 2 summarizes statistical analysis results with p values of each metric (cross correlation, bandwidth, and H_2 norm) according to trajectory type. Statistically significant results are marked with $\star$.

The participants achieved the best tracking accuracy with the ideal global view (IGV) for all three trajectories, while the worst performance occurred with the real local view (RLV), as we expected, except for the case of the y-

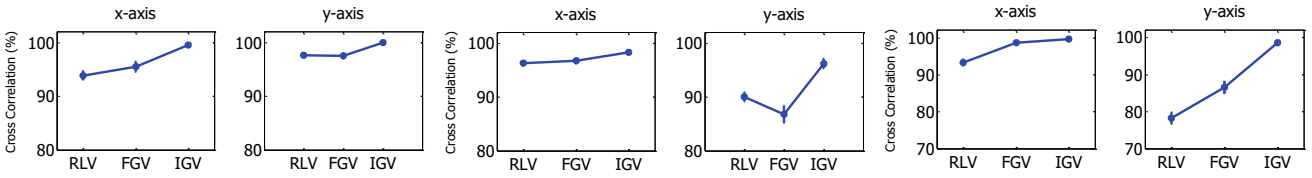

Fig. 9 Maneuverability performance for cross-correlation of the position tracking $CC_{position}$ (in percent). **a** The straight trajectory. **b** The semicircular trajectory. **c** The sinusoidal trajectory. RLV, FGV, and IGV represent real local view, fabricated global view, and ideal global view feedbacks, respectively

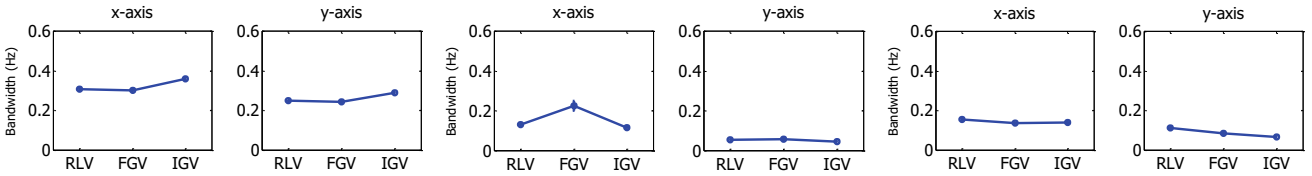

Fig. 10 Maneuverability performance for bandwidth of the maneuverability ω_{bd}. **a** The straight trajectory. **b** The semicircular trajectory. **c** The sinusoidal trajectory. RLV, FGV, and IGV represent real local view, fabricated global view, and ideal global view feedbacks, respectively

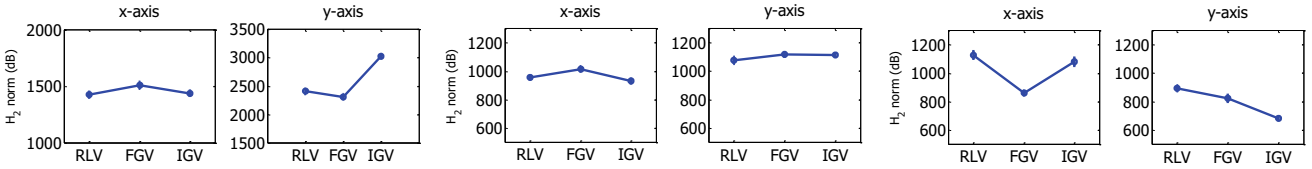

Fig. 11 Maneuverability performance for the H_2 norm of the maneuverability $\|\Phi_{maneuv}\|_2$. **a** The straight trajectory. **b** The semicircular trajectory. **c** The sinusoidal trajectory. RLV, FGV, and IGV represent real local view, fabricated global view, and ideal global view feedbacks, respectively

Table 2 ANOVA test results in the maneuvering test

Trajectory	p value					
	Cross correlation		Bandwidth		H_2 norm	
	x-axis	y-axis	x-axis	y-axis	x-axis	y-axis
Straight	0.3359	0.3443	0.3173	0.0654	0.8497	0.0126⋆
Semicircular	0.6389	0.3593	0.3502	0.6514	0.6637	0.9175
Sinusoidal	0.0220⋆	0.0214⋆	0.5624	0.2160	0.1517	0.1805

axis of the semicircular trajectory. Via the ANOVA test, the IGV of the sinusoidal trajectory has statistical significance ($p < 0.05$) which shows better performance of tracking accuracy. On the other hand, it cannot be concluded that the fabricated global view (FGV) has worse tracking performance than the IGV for the other trajectories.

In maneuverability, from the bandwidth (i.e., tracking accuracy with control effort) perspective, the IGV showed the best performance while the RLV showed the worst with the straight trajectory. With the semicircular trajectory, however, the FGV showed better performance than the IGV. In the case of the sinusoidal trajectory, the bandwidth performance for the three visual feedback methods showed small differences. Using the ANOVA test, the RLV, FGV, and IGV were proven not to show statistical performance differences, but the bandwidth y-axis showed statistical significance ($p = 0.0654$), close to 0.05.

Finally, it is noticeable that from the H_2 norm (i.e., tracking sensitivity) perspective, any visual feedback method did not contribute consistently to enhancing maneuverability, as shown in Fig. 11. However, for the case of the y-axis for the straight trajectory, the H_2 norm was increased when the IGV was used. As expected, the visual feedback methods were shown not to increase the performance of bandwidth except for the y-axis of the straight trajectory, which showed that the H_2 norm of the IGV was higher than either the RLV or FGV with the statistical significance ($p < 0.05$).

6.1.2 Situational awareness

Figure 12 shows task-dependent performance in the searching test, and Table 3 summarizes the results of the statistical ANOVA test for the five measures (P_{CT}, P_{CA}, P_{SO}, P_{SR}, and P_{TP}). In the test, the time limit was 10 min. Subjects took 7.68 min on average to complete the experi-

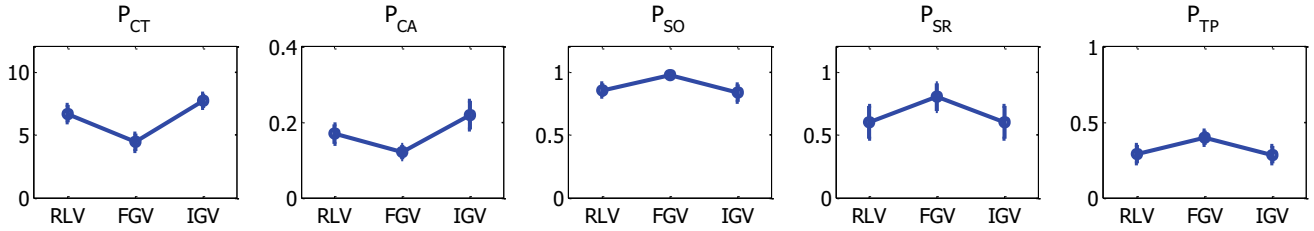

Fig. 12 Situational awareness performance of P_{CT}, P_{CA}, P_{SO}, P_{SR}, and P_{TP}. RLV, FGV, and IGV represent the real local view, fabricated global view, and ideal global view feedbacks, respectively

Table 3 ANOVA test results on the searching test

Comparison case	p value				
	P_{CT}	P_{CA}	P_{SO}	P_{SR}	P_{TP}
RLV and FGV and IGV	0.0039⋆	0.0681	0.1231	0.4243	0.2722
RLV and FGV	0.0298⋆	0.1516	0.0365⋆	0.2467	0.1666
FGV and IGV	0.0013⋆	0.0305⋆	0.0590	0.2467	0.1485

ment with the IGV. This is 72.2 % slower than with the FGV and 14.8 % slower than with the RLV ($\overline{P}_{CT}^{RLV} = 6.69$ min, $\overline{P}_{CT}^{FGV} = 4.46$ min, $\overline{P}_{CT}^{IGV} = 7.68$ min). This result means that, with the IGV, subjects needed more time to complete the task by controlling the multi-UAV system. However, the FGV showed the fastest performance in P_{CT}. Via the ANOVA test, it was shown that the FGV required less completion time statistically ($p < 0.01$).

Area coverage performance, P_{CA}, was below 0.25 with all visual feedback methods; this shows that less than about 25 % of the space was explored with the multi-UAV system ($\overline{P}_{CA}^{RLV} = 0.17, \overline{P}_{CA}^{FGV} = 0.12, \overline{P}_{CA}^{IGV} = 0.22$). Thus, the reward for large coverage area was zero. Even though participants completed the searching test within the time limit P_{CA} (i.e., found all objects) was lower than expected. This result could indicate that the searching test is more oriented towards the perception task than the navigation task (see Sect. 5.2). The ANOVA test showed that IGV had larger convergence than the FGV with statistical significance ($p < 0.05$), but it was also shown that the IGV did not contribute much to increasing area covered compared with the RLV.

The participants searched 16.9 and 14.1 % more objects with the FGV than with the IGV and RLV, respectively ($\overline{P}_{SO}^{RLV} = 0.85, \overline{P}_{SO}^{FGV} = 0.97, \overline{P}_{SO}^{IGV} = 0.83$). As expected, the FGV was shown to have better performance in searching for objects than the IGV, with statistical significance ($p < 0.05$).

Among the three feedback methods, the FGV showed the best performance in terms of safe return (P_{SR}). Except for the FGV, only about 60 % of the participants completed the searching test within the time limit. Otherwise, they failed to find all objects in the search space or the multi-UAV system crashed into the wall ($\overline{P}_{SR}^{RLV} = 0.60, \overline{P}_{SR}^{FGV} = 0.80, \overline{P}_{SR}^{IGV} = 0.60$). The statistical results, however, did not show that the FGV had better performance in P_{SR} than the RLV and IGV.

Unifying these metrics, task performance, P_{TP} was computed with the task-dependent metrics above and with normalizing factors. Figure 12 shows that participants performed 39.9 and 37.4 % better with the FGV than the IGV and RLV, respectively ($\overline{P}_{TP}^{RLV} = 0.29, \overline{P}_{TP}^{FGV} = 0.40, \overline{P}_{TP}^{IGV} = 0.29$). As we expected from the results, the FGV showed the best situational awareness. Note that P_{TP} was designed to include all metrics, participants' time management ability, perception of objects, and safety control of robots. However, the statistical results showed that the differences among those three values were not enough to show that FGV has better task performance.

6.2 Discussion

6.2.1 Effect of global view feedback

In all tests (i.e., maneuverability and situational awareness), the RLV feedback showed the worst performances. These results clearly show that there is a benefit to human operator's performance when using global view feedback in the teleoperation of multiple mobile robots in outdoor environments.

In particular, the IGV feedback, which is usually available from an external camera, contributes most to controlling the multi-robot system accurately and easily. With the FGV, on the other hand, human operators could be more aware of remote environments, enabling them to perform a specific task (e.g., search for objects) in a better way. This can be explained from the fact that there are both (real) local view and (fabricated) global view feedbacks in the FGV, unlike the IGV, so that human operators can be more aware of remote environments with additional information and maneuver the multi-robot system more accurately and easily.

6.2.2 Global localization

Although the FGV feedback is helpful for increasing a human operator's situational awareness in outdoor environments, there is still a need for global localization in order to increase the quality of the global view feedback; this could be solved by using an additional sensor (e.g., global positioning system).

Human operators may use an environment for the global localization of the multi-robots [34]. For example, someone could organize a global map of the multi-robot system and its environments by overlapping environment information captured from on-board cameras in a cognitive way. Therefore, the quality of the FGV could be also enhanced by incorporating information about the environment with that of the multi-robot system (e.g., simultaneous localization and mapping).

7 Conclusion

In this paper, we proposed a multi-modal feedback method with visual and force feedback for multi-robot teleoperation in outdoor environments. To overcome the limitations of global localization/information in outdoor environments, visual feedback was proposed by fabricating the formation information of the multi-robot system as global view feedback from local view feedback captured from on-board cameras. In addition, force feedback was added to make human operator of inertia information for the multi-UAV system by transmitting the difference between the commanded and actual velocities. As a preliminary study, only the proposed visual feedback method was evaluated using two psychophysical experiments, maneuvering and searching tests, from a human-centered performance perspective, i.e., maneuverability and situational awareness.

The ideal global visual feedback showed the best performance in trajectory tracking and maneuverability from the bandwidth perspective, but tracking sensitivity was not affected significantly by any visual feedback methods. The proposed fabricated global view feedback demonstrated the best performance in terms of situational awareness.

Acknowledgements This research was supported in part by the Max Planck Society, in part by Basic Science Research Program through the National Research Foundation of Korea (NRF) funded by the Ministry of Science, ICT and Future Planning under Grant NRF-2015R1C1A1A02036875, in part by Chonnam National University (2015-0536), and in part by a Grant (115062-2) funded by the Ministry of Agriculture, Food and Rural Affairs (MAFRA, Korea).

References

1. Murray R (2007) Recent research in cooperative control of multivehicle systems. J Dyn Syst Meas Control 129:571–583
2. Lee D, Spong M (2005) Bilateral teleoperation of multiple cooperative robots over delayed communication networks: theory. In: IEEE Int Conf Robot Autom, pp 360–365
3. Franchi A, Secchi C, Son HI, Bülthoff HH, Giordano PR (2012) Bilateral teleoperation of groups of mobile robots with time-varying topology. IEEE Trans Robot 28(5):1019–1033
4. Lee D, Franchi A, Son HI, Ha C, Bülthoff H, Giordano PR (2013) Semiautonomous haptic teleoperation control architecture of multiple unmanned aerial vehicles. IEEE ASME Trans Mechatron 18(4):1334–1345
5. Son HI, Franchi A, Chuang LL, Kim J, Bülthoff HH, Giordano PR (2013) Human-centered design and evaluation of haptic cueing for teleoperation of multiple mobile robots. IEEE Trans Cybern 43(2):597–609
6. Zhang J, Liu W, Wu Y (2011) Novel technique for vision-based UAV navigation. IEEE Trans Aerosp Electron Syst 47(4):2731–2741
7. Lam T, Mulder M, Paassen v (2007) Haptic interface for UAV collision avoidance. Int J Aviat Psychol 17(2):167–195
8. Son HI, Chuang L, Kim J, Bülthoff H (2011) Haptic feedback cues can improve human perceptual awareness in multi-robots teleoperation. In: Int conf on control, automation and systems, pp 1323–1328
9. Chen JY, Barnes MJ, Harper-Sciarini M (2011) Supervisory control of multiple robots: human-performance issues and user-interface design. IEEE Trans Syst Man Cybern C Appl Rev 41(4):435–454
10. Labonte D, Boissy P, Michaud F (2010) Comparative analysis of 3-d robot teleoperation interfaces with novice users. IEEE Trans Syst Man Cybern B Cybern 40(5):1331–1342
11. Pitman D (2010) Collaborative micro aerial vehicle exploration of outdoor environments. PhD Thesis, Massachusetts Institute of Technology
12. Giordano P, Deusch H, Lächele J, Bülthoff HH (2010) Visual-vestibular feedback for enhanced situational awareness in teleoperation of UAVs. In: AHS annual forum and technology display, pp 1–10
13. Son HI, Kim J, Chuang L, Franchi A, Robuffo Giordano P, Lee D, Bülthoff H (2011) An evaluation of haptic cues on the teleoperator's perceptual awareness of multiple UAVs' environments. In: World haptics conference, pp 149–154
14. Son HI, Chuang LL, Franchi A, Kim J, Lee D, Lee S.-W., Bülthoff HH, Robuffo Giordano P (2011) Measuring an operator's maneuverability performance in the haptic teleoperation of multiple robots. In: IEEE/RSJ int conf on intelligent robots and systems, pp 3039–3046
15. Mast M, Španěl M, Arbeiter G, Štancl V, Materna Z, Weisshardt F, Burmester M, Smrž P, Graf B (2013) Teleoperation of domestic service robots: effects of global 3d environment maps in the user interface on operators' cognitive and performance metrics. In: Social robotics. Springer, pp 392–401
16. Nielsen C, Goodrich M, Ricks R (2007) Ecological interfaces for improving mobile robot teleoperation. IEEE Trans Robot 23(5):927–941
17. Kelly A, Chan N, Herman H, Huber D, Meyers R, Rander P, Warner R, Ziglar J, Capstick E (2011) Real-time photorealistic virtualized reality interface for remote mobile robot control. Int J Rob Res 30(3):384–404
18. Steinfeld A, Fong T, Kaber D, Lewis M, Scholtz J, Schultz A, Goodrich M (2006) Common metrics for human-robot interaction. In: ACM SIGCHI/SIGART conf on human–robot interaction, pp 33–40
19. Saleh JA, Karray F (2011) Towards unified performance metrics for multi-robot human interaction systems. In: Autonomous and intelligent systems. Springer, pp 311–320

20. Gatsoulis Y, Virk GS, Dehghani-Sanij AA (2010) On the measurement of situation awareness for effective human–robot interaction in teleoperated systems. J Cogn Eng Decis Mak 4(1):69–98
21. Lee DG, Cho GR, Lee MS, Kim B-S, Oh S, Son HI (2013) Human-centered evaluation of multi-user teleoperation for mobile manipulator in unmanned offshore plants. In: IEEE/RSJ int conf on intelligent robots and systems, pp 5431–5438
22. Schreckenghost D, Milam T, Fong T (2010) Measuring performance in real time during human-robot operations with adjustable autonomy. IEEE Intell Syst 25:36–45
23. Nisky I, Mussa-Ivaldi FA, Karniel A (2013) Analytical study of perceptual and motor transparency in bilateral teleoperation. IEEE Trans Hum Mach Syst 43(6):570–581
24. Glas DF, Kanda T, Ishiguro H, Hagita N (2012) Teleoperation of multiple social robots. IEEE Trans Syst Man Cybern A Syst Hum 42(3):530–544
25. Franchi A, Masone C, Grabe V, Ryll M, Bülthoff HH, Giordano PR (2012) Modeling and control of UAV bearing formations with bilateral high-level steering. Int J Rob Res 31(12):1504–1525
26. Hong A, Bülthoff HH, Son HI (2013) A visual and force feedback for multi-robot teleoperation in outdoor environments: a preliminary result. In: IEEE int conf robot autom, pp 1471–1478
27. Franchi A, Masone C, Bülthoff HH, Giordano PR (2011) Bilateral teleoperation of multiple uavs with decentralized bearing-only formation control. In: IEEE/RSJ int conf on intelligent robots and systems. IEEE, pp 2215–2222
28. Ryu J, Kim Y, Hannaford B (2004) Sampled-and continuous-time passivity and stability of virtual environments. IEEE Trans Robot 20(4):772–776
29. Lee D, Huang K (2010) Passive-set-position-modulation framework for interactive robotic systems. IEEE Trans Robot 26(2):354–369
30. Franken M, Stramigioli S, Misra S, Secchi C, Macchelli A (2011) Bilateral telemanipulation with time delays: a two-layer approach combining passivity and transparency. IEEE Trans Robot 27(4):741–756
31. Experiment Database, Max Planck Campus Tübingen. https://experiments.tuebingen.mpg.de/
32. Lächele J (2011) Development of a real-time simulation environment for multiple robot systems. Diploma Thesis, Eberhard Karls Universität Tübingen
33. Gescheider GA (1997) Psychophysics: the fundamentals. Lawrence Erlbaum Associates, Mahwah, New Jersey
34. Velagapudi P, Owens S, Scerri P, Sycara K, Le M (2009) Environmental factors affecting situation awareness in unmanned aerial vehicles. In: AIAA conf, pp 1–7